Engineering Analysis with Boundary Elements 122 (2021) 75–84

Contents lists available at ScienceDirect

Engineering Analysis with Boundary Elements

journal homepage: www.elsevier.com/locate/enganabound

A dual interpolation precise integration boundary face method to solve two-dimensional transient heat conduction problems

Le Yang, Jianming Zhang*, Rui He, Weicheng Lin

State Key Laboratory of Advanced Design and Manufacturing for Vehicle Body, College of Mechanical and Vehicle Engineering, Hunan University, Changsha 410082, China

ARTICLE INFO

Keywords:
Dual interpolation method
Precise integration method
Moving least-squares approximation
Matrix exponential function
Transient heat conduction

ABSTRACT

In this paper, we present a new numerical algorithm combining the dual interpolation boundary face method (DiBFM) with the precise integration method for solving the 2D transient heat conduction problem. In this new combined approach, the transient heat conduction problem is transformed from an initial boundary value problem to an initial value problem through a dual interpolation boundary face approach. This approach merges the conforming and nonconforming elements in the BFM implementation. Potentials and fluxes are approximated by the dual interpolation elements which include source and virtual points. Employing the moving-least-square approximation help to construct the constraint equations relating to virtual points. Then the analytical solution of the problem can be expressed by the matrix exponential function (MEF), which can be computed accurately through a precise integration method (PIM). The proposed numerical algorithm has been successfully implemented. Several numerical examples are given to illustrate the numerical accuracy and stability of the proposed method compared with the traditional precise integration boundary face method.

1. Introduction

One of the most common practical problems is the transient heat transfer problem. The current numerical calculation methods for this problem include the finite difference method (FDM) [1], the finite volume method (FVM) [2], the finite element method (FEM) [3], the boundary element method (BEM) [4] and the boundary face method (BFM) [5].In these numerical tools, the BEM is more superior to others for its semi-analytical feature and advantage in using the discontinuous elements. This makes the numerical results more accurate and the mesh generation a less time-consuming and effective process. The same as BEM, BFM is developed on the basis of the boundary integral equation (BIE), but by making full use of the boundary representation data structure in the Computer Aided Design (CAD) package directly, the computational model inherits all geometric data from CAD geometries.

In macroscopic level, the BEM implementation of transient heat conduction problem is categorized into two kinds: the transformed domain method [6-7] and the time domain method [8-10]. The transformed domain schemecan yield higher computational accuracy, however, there are two defects in this method: (i) The numerical inverse Laplace transformation is not conducive to large-scale calculation, for it requires much more computational efforts; (ii) The accuracy of the result depends on the determination of transformation parameters. Hence the transformed domain method's application and promotion is very difficult.

In this paper, the time domain method is studied. The time domain methods can be further subdivided into two categories: In one category of this numerical scheme, the time-independent fundamental solution, which is usually used to solve steady-state heat transfer problems, is employed, and the other one implements with the time-dependent fundamental solution. The numerical approach applying the time-dependent fundamental solution was proposed by Thaler et al. [11], Brebbia [12] classified this approach into two numerical algorithms: convolution quadrature method (CQM) and quasi-initial condition method, respectively. CQM's each step of calculation needs to consider physical variables from initial time to current time step. While in quasi-initial condition method, the present moment's numerical result only considers the previous time step's physical variable which is used as the initial boundary condition in the current time step.

In the numerical approach with time-independent fundamental solution, Zhou firstly takes the transient heat transfer problem as a quasi-steady state problem, and the time derivativeis treated as the equivalent heat source [13]. In Zhou's work, the transient heat transfer problem is transformed from an initial boundary value problem into an initial value problem through a dual reciprocity boundary element algorithm which implements with the steady-state fundamental solution, the PIM, which

* Corresponding author.
E-mail address: zhangjianm@gmail.com (J. Zhang).

https://doi.org/10.1016/j.enganabound.2020.09.014
Received 15 June 2020; Received in revised form 27 August 2020; Accepted 13 September 2020
Available online 24 October 2020

Nomenclature

ξ, η	The local natural coordinates of a 2D dual interpolation element
d	Offset
n_α	The number of source points in the dual interpolation element
n_β	The number of virtual points in the dual interpolation element
$N_\alpha^s(\xi)$	Shape function of the α^{th} source point in the dual interpolation element
$u(Q_\alpha^s)$	Potential of the α^{th} source point in the dual interpolation element
$q(Q_\alpha^s)$	Normal flux of the α^{th} source point in the dual interpolation element
$N_\beta^v(\xi)$	Shape function of the β^{th} source point in the dual interpolation element
$u(Q_\beta^v)$	Potential of the β^{th} source point in the dual interpolation element
$q(Q_\beta^v)$	Normal flux of the β^{th} source point in the dual interpolation elemen
M^β	The number of source points that are within the influential area of virtual point
$\phi_m^{vs}(\xi_\beta^v)$	The MLS interpolation shape function affiliated with source point
ξ_β^v	The parameter space's coordinate of virtual point
Γ_u	The boundary of Dirichlet type
Γ_q	The boundary of Neumann type
$\bar{u}(\mathbf{x},t)$	Prescribed temperature on Γ_u
$\bar{q}(\mathbf{x},t)$	Prescribed normal flux on Γ_q
$u_0(\mathbf{x})$	Prescribed temperature in 2-D domain Ω at initial time
$\dot{u}(\mathbf{x},t)$	The first derivatives of the $u(\mathbf{x},t)$versus time variable t
$u^*(\mathbf{y},\mathbf{x})$	The time-independent fundamental solution
$k\frac{\partial u^*(\mathbf{y},\mathbf{x})}{\partial n(\mathbf{x})}$	The derivative of $u^*(\mathbf{y},\mathbf{x})$versus normal vector n
Q	The heat source inside the considered domain
k	Heat conductivity
ρ	Density
c	Heat capacity
$\mathbf{\Psi}_{nn}^{vs}$,$\mathbf{\Theta}_{dd}^{vs}$,$\mathbf{\Phi}^{vs}$	Shape function matrices acquired by the MLS approximation
Δt	Time step length

is firstly presented by Zhong et al. to solve structural dynamics [14], is eventually employed to calculate the initial value problem accurately.

The recently proposed dual interpolation boundary face method (DiBFM) [15-18] has been demonstrated the higher accuracy and efficiency compared with the traditional boundary element method. Those advantages are mainly based on two reasons: (i) Compared to conventional discontinuous elements, the dual interpolation elements in DiBFM improve the interpolation accuracy by two orders. (ii) DiBFM eliminate geometry error since the integrand quantities are calculated directly from the curves rather than from elements. In this new proposed algorithm, the boundary physical variables are interpolated by the dual interpolation elements which contains source points and virtual points. In addition, it should be mentioned that we employ the MLS approximation to construct the constraint equations relating to virtual points. Thus, compared with the traditional BEM, the DiBFM largely improves the accuracy and efficiency. Considering the advantages of the precise integration method [13] in accuracy and stability, it is natural to extend this scheme to the dual interpolation BFM.

In this paper, we present a new numerical scheme combining the dual interpolation boundary face method (DiBFM) with the precise integration method for solving the 2D transient heat conduction problem. This paper's primary contributions are as follows: (i) While satisfy the precondition of the same time step, this new method is more accurate than the traditional precise integration boundary face method; (ii) unlike the numerical method with time-dependent fundamental solution which has the numerically instability phenomenon, this coupled method still exhibits accuracy and stability when the time step length becomes smaller and smaller.

The article is divided into six sections: In Section 2, we describe the dual interpolation method with MLS approximation. In Section 3, the equations of the DiBFM for transient heat conduction problems are presented. In Section 4, we describe the PIM for previous section's equation in detail. In Section 5, results of several numerical examples are given to illustrate the superiority of the proposed method in dealing with 2-D transient heat conduction problems. In Section 6, we close with some discussions and conclusions.

2. Dual interpolation method with MLS approximation

The first-layer interpolation for boundary variables and the second-layer interpolation for virtual points are introduced in this section.

2.1. Dual interpolation element

The DiBFM's elements shown in Figs. 1 and 2 are called the 2D dual interpolation element. This new interpolation element contains the source (s_i) and virtual (v_i) points. The virtual points help to improve the interpolation accuracy, however, they are not treated as the collocation points, and the degrees of freedom associated with this kind of points are compressed by constraint equations which are constructed through MLS approximation. Thus, the 2D dual interpolation elements have potentiality to unify the 2D continuous and discontinuous elements. The shape functions for S1, S2, S3 in Fig. 1 and TS1 in Fig. 2 are given by Eq. (1-3) and Eq. (4), the shape functions for TS2 and TS3 can be formulated in the same way as the standard elements of BEM.

S1, S2, S3 elements' shape functions:

$$N_1^s(\xi)=(1+\xi)(1-\xi) \text{ and } \begin{cases} N_1^v(\xi)=\dfrac{1}{2}\xi(\xi-1) \\ N_2^v(\xi)=\dfrac{1}{2}\xi(\xi+1) \end{cases} \tag{1}$$

$$\begin{cases} N_1^s(\xi)=\dfrac{[\xi-(1-d)](\xi+1)(\xi-1)}{2d(1-d)(2-d)} \\ N_2^s(\xi)=-\dfrac{[\xi+(1-d)](\xi+1)(\xi-1)}{2d(1-d)(2-d)} \end{cases} \text{ and}$$

$$\begin{cases} N_1^v(\xi)=-\dfrac{[\xi+(1-d)][\xi-(1-d)](\xi-1)}{2d(2-d)} \\ N_2^v(\xi)=\dfrac{[\xi+(1-d)][\xi-(1-d)](\xi+1)}{2d(2-d)} \end{cases} \tag{2}$$

$$\begin{cases} N_1^s(\xi)=-\dfrac{[\xi-(1-d)](\xi+1)(\xi-1)\xi}{2d(2-d)(1-d)^2} \\ N_2^s(\xi)=\dfrac{[\xi+(1-d)][\xi-(1-d)](\xi+1)(\xi-1)}{(1-d)^2} \\ N_3^s(\xi)=-\dfrac{[\xi+(1-d)](\xi+1)(\xi-1)\xi}{2d(2-d)(1-d)^2} \end{cases} \text{ and}$$

$$\begin{cases} N_1^v(\xi)=\dfrac{[\xi+(1-d)][\xi-(1-d)](\xi-1)\xi}{2d(2-d)} \\ N_2^v(\xi)=\dfrac{[\xi+(1-d)][\xi-(1-d)](\xi+1)\xi}{2d(2-d)} \end{cases} \tag{3}$$

The independent variable ξ denotes the local natural coordinates of a 2D dual interpolation element, and the upper and lower bounds of ξ is

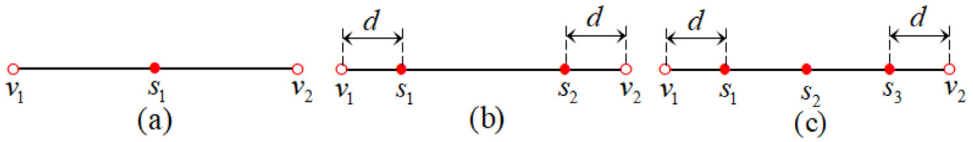

Fig. 1. The 2D dual interpolation line elements: (a) S1, (b) S2, and (c) S3.

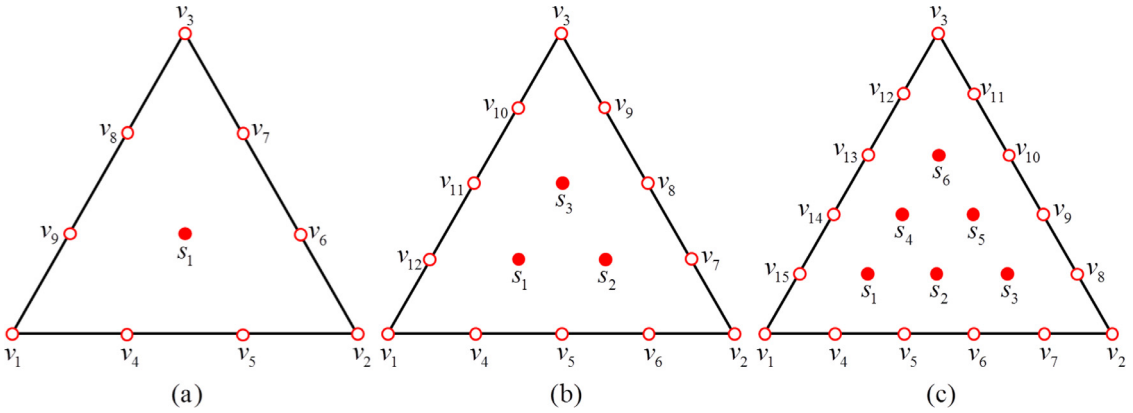

Fig. 2. The 2D dual interpolation triangle elements: (a) TS1, (b) TS2, and (c) TS3.

$[-1,1]$, where the offset d is taken to be $\frac{1}{4}$in this paper, the offset d is an empirical data, according to Ref. [19], the 'best' parameter d should be between 0.2 and 0.25. The details of these shape functions, which are composed of Lagrangian interpolation formulation, can be found in the previous work in Ref. [19].

TS1 element's shape function:

$$\left\{N_1^s(\xi,\eta)=27\xi\eta(1-\xi-\eta)\quad\text{and}\right.$$

$$\begin{cases} N_1^v(\xi,\eta)=0.5(3\xi-1)(3\xi-2)\xi \\ N_2^v(\xi,\eta)=0.5(3\eta-1)(3\eta-2)\eta \\ N_3^v(\xi,\eta)=0.5(2-3\xi-3\eta)(1-3\xi-3\eta)(1-\xi-\eta) \\ N_4^v(\xi,\eta)=4.5\xi\eta(3\xi-1) \\ N_5^v(\xi,\eta)=4.5\xi\eta(3\eta-1) \\ N_6^v(\xi,\eta)=4.5\eta(1-\xi-\eta)(3\eta-1) \\ N_7^v(\xi,\eta)=4.5\eta(1-\xi-\eta)(2-3\xi-3\eta) \\ N_8^v(\xi,\eta)=4.5\xi(1-\xi-\eta)(2-3\xi-3\eta) \\ N_9^v(\xi,\eta)=4.5\xi(1-\xi-\eta)(3\xi-1) \end{cases} \tag{4}$$

The independent variable ξ and η denote the local natural coordinates, and the upper and lower bounds of ξ and η is [0,1].

2.2. First-layer interpolation for boundary variables

For two-dimensionaltransient heat transfer problem, the boundary physical variables u and q are interpolated by 2D dual interpolation element (first-layer interpolation):

$$u(x_1,x_2)=u(\xi)=\sum_{\alpha=1}^{n_\alpha}N_\alpha^s(\xi)u(Q_\alpha^s)+\sum_{\beta=1}^{n_\beta}N_\beta^v(\xi)u(Q_\beta^v), \tag{5}$$

$$q(x_1,x_2)=q(\xi)=\sum_{\alpha=1}^{n_\alpha}N_\alpha^s(\xi)q(Q_\alpha^s)+\sum_{\beta=1}^{n_\beta}N_\beta^v(\xi)q(Q_\beta^v), \tag{6}$$

where n_α and n_β are the number of source and virtual points in the dual interpolation element. $N_\alpha^s(\xi)$, $u(Q_\alpha^s)$and $q(Q_\alpha^s)$are the shape function, potential and normal flux of the α^{th} source point in the dual interpolation element. $N_\beta^v(\xi)$, $u(Q_\beta^v)$and $q(Q_\beta^v)$are the shape function, potential and flux of the β^{th} virtual point. In this paper, the virtual nodal parameters $u(Q_\beta^v)$and $q(Q_\beta^v)$are dependent on physical variables of source points, MLS is employed for the second layer approximation to construct their relations.

2.3. Second-layer interpolation for virtual nodes

We use the MLS approximation to obtain the u and q of virtual points. The physical variables u and q of virtual points are approximated as follows:

$$u\left(Q_\beta^v\right)=\sum_{m=1}^{M^\beta}\phi_m^{vs}\left(\xi_\beta^v\right)u\left(Q_{m(\beta)}^s\right), \tag{7}$$

$$q\left(Q_\beta^v\right)=\sum_{m=1}^{M^\beta}\phi_m^{vs}\left(\xi_\beta^v\right)q\left(Q_{m(\beta)}^s\right), \tag{8}$$

where M^βdenotes the number of source points $Q_{m(\beta)}^s$that are within the influential area of virtual point Q_β^v, $\phi_m^{vs}(\xi_\beta^v)$is the MLS interpolation shape function affiliated with source point $Q_{m(\beta)}^s$, $u(Q_{m(\beta)}^s)$and $q(Q_{m(\beta)}^s)$are temperature and normal flux of source point $Q_{m(\beta)}^s$, and the $\xi_\beta^v$is the parameter space's coordinate of virtual point Q_β^v. The details of the MLS approximation and the interpolation functions in Eqs. (7), (8) can be found in the previous work in Ref. [19]and Ref. [20].

Substituting Eq. (7) into Eq. (5) leads to the equation of the temperature u:

$$u(\xi)=\sum_{\alpha=1}^{n\alpha}N_\alpha^s(\xi)u\left(Q_\alpha^s\right)+\sum_{\beta=1}^{n\beta}\sum_{m=1}^{M^\beta}N_\beta^v(\xi)\phi_m^{vs}\left(\eta_\beta^v\right)u\left(Q_{m(\beta)}^s\right) \tag{9}$$

and substituting Eq. (8) into Eq. (6) leads to the equationof the normal flux q:

$$q(\xi)=\sum_{\alpha=1}^{n\alpha}N_\alpha^s(\xi)q\left(Q_\alpha^s\right)+\sum_{\beta=1}^{n\beta}\sum_{m=1}^{M^\beta}N_\beta^v(\xi)\phi_m^{vs}\left(\eta_\beta^v\right)q\left(Q_{m(\beta)}^s\right) \tag{10}$$

3. DiBFM for transient heat conduction problem

Consider the transient heat conduction problem in the 2-D domain Ω which is enclosed by the boundary $\Gamma=\Gamma_u+\Gamma_q$. The problem in homogeneous media is expressed as:

$$\begin{aligned} &\frac{k}{\rho c}\nabla^2u(\mathbf{x},t)+\frac{Q(\mathbf{x},t)}{\rho c}=\dot{u}(\mathbf{x},t), && \forall x\in\Omega \\ &u(\mathbf{x},t)=\bar{u}(\mathbf{x},t), && \forall x\in\Gamma_u \\ &k\frac{\partial u(\mathbf{x},t)}{\partial n(\mathbf{x})}\equiv q(\mathbf{x},t)=\bar{q}(\mathbf{x},t), && \forall x\in\Gamma_q \\ &u\left(\mathbf{x},t_0\right)=u_0(\mathbf{x}), && \forall x\in\Omega \end{aligned} \tag{11}$$

where Γ_u is the boundary of Dirichlet type, Γ_q is the boundary of Neumann type, $\bar{u}(\mathbf{x},t)$is prescribed temperature on Γ_u, $\bar{q}(\mathbf{x},t)$is prescribed normal flux on Γ_q, $u_0(\mathbf{x})$ is prescribed temperature in 2-D domain Ω at initial time, $\dot{u}(\mathbf{x},t)$stands for the first derivatives of the $u(\mathbf{x}, t)$versus time variable t.

In the BEM, by the aid of the time-independent fundamental solution of a 2-D steady state potential problem, the governing equation of heat conduction problem can be transformed into the following boundary integral form:

$$c(\mathbf{y})u(\mathbf{y}) + \frac{1}{\rho c}\int_\Gamma \left(k\frac{\partial u^*(\mathbf{y},\mathbf{x})}{\partial n(\mathbf{x})}\right)u(\mathbf{x},t)d\Gamma(\mathbf{x}) = \frac{1}{\rho c}\int_\Gamma u^*(\mathbf{y},\mathbf{x})\left(k\frac{\partial u(\mathbf{x},t)}{\partial n(\mathbf{x})}\right)d\Gamma(\mathbf{x}) + \frac{1}{\rho c}\int_\Omega u^*(\mathbf{y},\mathbf{x})Q(\mathbf{y},\mathbf{x})d\Omega(\mathbf{x}) - \int_\Omega u^*(\mathbf{y},\mathbf{x})\dot{u}(\mathbf{x},t)d\Omega(\mathbf{x}) \tag{12}$$

where the coefficient $c(\boldsymbol{y})$ is defined as:

$$c(\mathbf{y}) = \begin{cases} 1 & \text{y in the internal domain} \\ \frac{1}{2} & \text{y on the smooth boundary} \\ 0 & \text{y in the outer domain} \end{cases} \tag{13}$$

where $u(\mathbf{x}, t)$ and $k\frac{\partial u(\mathbf{x},t)}{\partial n(\mathbf{x})}$are the temperature and the normal flux at the boundary node $\boldsymbol{x}$.$u^*(\mathbf{y}, \mathbf{x})$ is the time-independent fundamental solution, and $k\frac{\partial u^*(\mathbf{y},\mathbf{x})}{\partial n(\mathbf{x})}$is the derivative of $u^*(\mathbf{y}, \mathbf{x})$ versus normal vector n. Q is the heat source inside the considered domain, k, ρ and c are heat conductivity, density and heat capacity of the material. For 2-D potential problems, $u^*(\mathbf{y}, \mathbf{x})$ and $q^*(\mathbf{y}, \mathbf{x})$ are given by:

$$\begin{aligned} u^*(\mathbf{y},\mathbf{x}) &= -\frac{\rho c}{2\pi k}\ln r \\ q^*(\mathbf{y},\mathbf{x}) &= k\frac{\partial u^*(\mathbf{y},\mathbf{x})}{\partial n(\mathbf{x})} \\ r &= |\mathbf{y}-\mathbf{x}| \end{aligned} \tag{14}$$

where r is the linear distance between the source node $\boldsymbol{y}$ and the field node $\boldsymbol{x}$.

In the DiBFM, the BIEs are only collocated at the source nodes, and the discretization form of the BIE for transient heat conduction problem is:

$$\begin{aligned} &c(\mathbf{y})u(\mathbf{y}) + \frac{1}{\rho c}\sum_j\left(\sum_{\alpha=1}^{n\alpha}\int_{\Gamma_j} q^*(\mathbf{y},\mathbf{x})u(\mathbf{x}^s_{j(\alpha)},t)N^s_{j(\alpha)}(\mathbf{x})d\Gamma(\mathbf{x}) + \sum_{\beta=1}^{n\beta}\int_{\Gamma_j} q^*(\mathbf{y},\mathbf{x})u(\mathbf{x}^v_{j(\beta)},t)N^v_{j(\beta)}(\mathbf{x})d\Gamma(\mathbf{x})\right) \\ &= \frac{1}{\rho c}\sum_j\left(\sum_{\alpha=1}^{n\alpha}\int_{\Gamma_j} u^*(\mathbf{y},\mathbf{x})q(\mathbf{x}^s_{j(\alpha)},t)N^s_{j(\alpha)}(\mathbf{x})d\Gamma(\mathbf{x}) + \sum_{\beta=1}^{n\beta}\int_{\Gamma_j} u^*(\mathbf{y},\mathbf{x})q(\mathbf{x}^v_{j(\beta)},t)N^v_{j(\beta)}(\mathbf{x})d\Gamma(\mathbf{x})\right) \\ &\quad + \frac{1}{\rho c}\sum_i\sum_m\int_{\Omega_i} u^*(\mathbf{y},\mathbf{x})Q(\mathbf{x}_m,t)N^s_m(\mathbf{x})d\Omega(\mathbf{x}) - \sum_i\sum_m\int_{\Omega_i} u^*(\mathbf{y},\mathbf{x})\dot{u}(\mathbf{x}_m,t)N^s_m(\mathbf{x})d\Omega(\mathbf{x}) \\ &\quad + \frac{1}{\rho c}\sum_i\sum_l\int_{\Omega_i} u^*(\mathbf{y},\mathbf{x})Q(\mathbf{x}_l,t)N^v_l(\mathbf{x})d\Omega(\mathbf{x}) - \sum_i\sum_l\int_{\Omega_i} u^*(\mathbf{y},\mathbf{x})\dot{u}(\mathbf{x}_l,t)N^v_l(\mathbf{x})d\Omega(\mathbf{x}) \end{aligned} \tag{15}$$

Then we collocate the BIEs at every source node on the boundary, andthe matrix form of the systems is expressed as:

$$\mathbf{Hu} = \mathbf{Gq} + \mathbf{SQ} - \mathbf{D}\dot{\mathbf{u}} \tag{16}$$

In order to make the derivation process lucid and agreed, we decompose the **H** and **G** in Eq. (16) according to the boundary conditions, one has:

$$\begin{bmatrix} \mathbf{H}^{ss}_{dd} & \mathbf{H}^{ss}_{dn} & \mathbf{H}^{sv}_{dd} & \mathbf{H}^{sv}_{dn} \\ \mathbf{H}^{ss}_{nd} & \mathbf{H}^{ss}_{nn} & \mathbf{H}^{sv}_{nd} & \mathbf{H}^{sv}_{nn} \end{bmatrix}\begin{Bmatrix} \bar{\mathbf{u}}^s_d \\ \mathbf{u}^s_n \\ \bar{\mathbf{u}}^v_d \\ \mathbf{u}^v_n \end{Bmatrix} = \begin{bmatrix} \mathbf{G}^{ss}_{dd} & \mathbf{G}^{ss}_{dn} & \mathbf{G}^{sv}_{dd} & \mathbf{G}^{sv}_{dn} \\ \mathbf{G}^{ss}_{nd} & \mathbf{G}^{ss}_{nn} & \mathbf{G}^{sv}_{nd} & \mathbf{G}^{sv}_{nn} \end{bmatrix}\begin{Bmatrix} \mathbf{q}^s_d \\ \bar{\mathbf{q}}^s_n \\ \mathbf{q}^v_d \\ \bar{\mathbf{q}}^v_n \end{Bmatrix} + [\mathbf{S}]_{\mathrm{BD}}\{\mathbf{Q}_{\mathrm{D}}\} - [\mathbf{D}^{ss}\mathbf{D}^{sv}]_{\mathrm{BD}}\begin{Bmatrix} \dot{\mathbf{u}}^s_{\mathrm{D}} \\ \dot{\mathbf{u}}^v_{\mathrm{D}} \end{Bmatrix} \tag{17}$$

where the subscripts d, n of the submatrices **H** and **G** represent the Dirichlet, Neumann boundary conditions, respectively, and the superscripts s, v denote the source node, virtual node. $\bar{u}$and $\bar{q}$are known potentials and fluxes. B, D stand for the number of the boundary source points and the number of the points inside the considered domain, respectively.

The unknown vectors $\mathbf{u}^v$, $\mathbf{q}^v$ and $\dot{\mathbf{u}}^v_{\mathrm{D}}$of virtual points is calculated by the MLS approximation. As a result, $\mathbf{u}^v$, $\mathbf{q}^v$ and $\dot{\mathbf{u}}^v_{\mathrm{D}}$can be expressed as follows:

$$\begin{aligned} \mathbf{u}^v_n &= \boldsymbol{\Psi}^{vs}_{nn}\mathbf{u}^s_n \\ \mathbf{q}^v_d &= \boldsymbol{\Theta}^{vs}_{dd}\mathbf{q}^s_d \\ \dot{\mathbf{u}}^v_{\mathrm{D}} &= \boldsymbol{\Phi}^{vs}\dot{\mathbf{u}}^s_{\mathrm{D}} \end{aligned} \tag{18}$$

where $\boldsymbol{\Psi}^{vs}_{nn}$, $\boldsymbol{\Theta}^{vs}_{dd}$ and $\boldsymbol{\Phi}^{vs}$ are shape function matrices acquired by the MLS approximation (see Section 2.3).

Substituting the approximations for $\mathbf{u}^v_n$and $\mathbf{q}^v_d$into Eq. (17) using Eq. (18), one gets:

$$\begin{bmatrix} \overline{\mathbf{H}}^{ss}_{dd} & \overline{\mathbf{H}}^{ss}_{dn} & \mathbf{H}^{sv}_{dd} \\ \overline{\mathbf{H}}^{ss}_{nd} & \overline{\mathbf{H}}^{ss}_{nn} & \mathbf{H}^{sv}_{nd} \end{bmatrix}\begin{Bmatrix} \bar{\mathbf{u}}^s_d \\ \mathbf{u}^s_n \\ \bar{\mathbf{u}}^v_d \end{Bmatrix} = \begin{bmatrix} \overline{\mathbf{G}}^{ss}_{dd} & \overline{\mathbf{G}}^{ss}_{dn} & \mathbf{G}^{sv}_{dn} \\ \overline{\mathbf{G}}^{ss}_{nd} & \overline{\mathbf{G}}^{ss}_{nn} & \mathbf{G}^{sv}_{nn} \end{bmatrix}\begin{Bmatrix} \mathbf{q}^s_d \\ \bar{\mathbf{q}}^s_n \\ \bar{\mathbf{q}}^v_n \end{Bmatrix} + [\mathbf{S}]_{\mathrm{BD}}\{\mathbf{Q}_{\mathrm{D}}\} - [\bar{\mathbf{D}}]_{\mathrm{BD}}\{\dot{\mathbf{u}}^s_{\mathrm{D}}\} \tag{19}$$

in which

$$\begin{bmatrix} \overline{\mathbf{H}}^{ss}_{dd} & \overline{\mathbf{H}}^{ss}_{dn} & \mathbf{H}^{sv}_{dd} \\ \overline{\mathbf{H}}^{ss}_{nd} & \overline{\mathbf{H}}^{ss}_{nn} & \mathbf{H}^{sv}_{nd} \end{bmatrix} = \begin{bmatrix} \mathbf{H}^{ss}_{dd} & \mathbf{H}^{ss}_{dn} & \mathbf{H}^{sv}_{dd} \\ \mathbf{H}^{ss}_{nd} & \mathbf{H}^{ss}_{nn} & \mathbf{H}^{sv}_{nd} \end{bmatrix} + \begin{bmatrix} \mathbf{0} & \mathbf{H}^{sv}_{dn}\boldsymbol{\Psi}^{vs}_{nn} & \mathbf{0} \\ \mathbf{0} & \mathbf{H}^{sv}_{nn}\boldsymbol{\Psi}^{vs}_{nn} & \mathbf{0} \end{bmatrix} \tag{20}$$

$$\begin{bmatrix} \overline{\mathbf{G}}^{ss}_{dd} & \overline{\mathbf{G}}^{ss}_{dn} & \mathbf{G}^{sv}_{dn} \\ \overline{\mathbf{G}}^{ss}_{nd} & \overline{\mathbf{G}}^{ss}_{nn} & \mathbf{G}^{sv}_{nn} \end{bmatrix} = \begin{bmatrix} \mathbf{G}^{ss}_{dd} & \mathbf{G}^{ss}_{dn} & \mathbf{G}^{sv}_{dn} \\ \mathbf{G}^{ss}_{nd} & \mathbf{G}^{ss}_{nn} & \mathbf{G}^{sv}_{nn} \end{bmatrix} + \begin{bmatrix} \mathbf{G}^{ss}_{dd}\boldsymbol{\Theta}^{vs}_{dd} & \mathbf{0} & \mathbf{0} \\ \mathbf{G}^{ss}_{nd}\boldsymbol{\Theta}^{vs}_{dd} & \mathbf{0} & \mathbf{0} \end{bmatrix} \tag{21}$$

$$[\bar{\mathbf{D}}]_{\mathrm{BD}} = [\mathbf{D}^{ss} + \mathbf{D}^{sv}\boldsymbol{\Phi}^{vs}]_{\mathrm{BD}} \tag{22}$$

By moving the known physical quantities to the right-hand side and unknown physical quantities to the left-hand side, finally, the discretized form of the BIE for transient heat transfer problem can be transformed into the following form:

$$\begin{Bmatrix} \mathbf{q}^s_d \\ \mathbf{u}^s_n \end{Bmatrix} = \mathbf{A}\begin{bmatrix} -\bar{\mathbf{H}}^{ss}_{dd} & \bar{\mathbf{G}}^{ss}_{dn} \\ -\bar{\mathbf{H}}^{ss}_{nd} & \bar{\mathbf{G}}^{ss}_{nn} \end{bmatrix}_{\mathrm{BB}}\begin{Bmatrix} \bar{\mathbf{u}}^s_d \\ \bar{\mathbf{q}}^s_n \end{Bmatrix} + \mathbf{A}\begin{bmatrix} -\mathbf{H}^{sv}_{dd} & \mathbf{G}^{sv}_{dn} \\ -\mathbf{H}^{sv}_{nd} & \mathbf{G}^{sv}_{nn} \end{bmatrix}\begin{Bmatrix} \bar{\mathbf{u}}^v_d \\ \bar{\mathbf{q}}^v_n \end{Bmatrix} + \mathbf{A}[\mathbf{S}]_{\mathrm{BD}}\{\mathbf{Q}_{\mathrm{D}}\} - \mathbf{A}[\bar{\mathbf{D}}]_{\mathrm{BD}}\{\dot{\mathbf{u}}_{\mathrm{D}}\}$$

$$\mathbf{A} = \begin{bmatrix} -\bar{\mathbf{G}}^{ss}_{dd} & \bar{\mathbf{H}}^{ss}_{dn} \\ -\bar{\mathbf{G}}^{ss}_{nd} & \bar{\mathbf{H}}^{ss}_{nn} \end{bmatrix}^{-1}_{\mathrm{BB}} \tag{23}$$

Then we collocate the BIEs at every source pointthat locates inside the considered domain, and the matrix form of the systems can be expressed as:

$$\begin{bmatrix}\mathbf{H}_{Dd}^{ss} & \mathbf{H}_{Dn}^{ss} & \mathbf{H}_{Dd}^{sv} & \mathbf{H}_{Dn}^{sv}\end{bmatrix}\begin{Bmatrix}\bar{\mathbf{u}}_d^s\\ \mathbf{u}_n^s\\ \bar{\mathbf{u}}_d^v\\ \mathbf{u}_n^v\end{Bmatrix}-\begin{bmatrix}\mathbf{G}_{Dd}^{ss} & \mathbf{G}_{Dn}^{ss} & \mathbf{G}_{Dd}^{sv} & \mathbf{G}_{Dn}^{sv}\end{bmatrix}\begin{Bmatrix}\mathbf{q}_d^s\\ \bar{\mathbf{q}}_n^s\\ \mathbf{q}_d^v\\ \bar{\mathbf{q}}_n^v\end{Bmatrix}+\mathbf{u}_{\mathrm{D}}$$
$$=[\mathbf{S}]_{\mathrm{DD}}\{\mathbf{Q}_{\mathrm{D}}\}-[\mathbf{D}^{ss}\mathbf{D}^{sv}]_{\mathrm{DD}}\begin{Bmatrix}\dot{\mathbf{u}}_{\mathrm{D}}^s\\ \dot{\mathbf{u}}_{\mathrm{D}}^v\end{Bmatrix} \tag{24}$$

Similarly, substituting the approximations for $\mathbf{u}_n^v$, $\mathbf{q}_d^v$and the described boundary conditions $\bar{\mathbf{u}}_d^v$, $\bar{\mathbf{q}}_n^v$of virtual nodes into the Eq. (24), we will have the following equation:

$$\begin{bmatrix}-\bar{\mathbf{G}}_d^{ss} & \bar{\mathbf{H}}_n^{ss}\end{bmatrix}_{\mathrm{DB}}\begin{Bmatrix}\mathbf{q}_d^s\\ \mathbf{u}_n^s\end{Bmatrix}$$
$$=\begin{bmatrix}-\bar{\mathbf{H}}_d^{ss} & \bar{\mathbf{G}}_n^{ss}\end{bmatrix}_{\mathrm{DB}}\begin{Bmatrix}\bar{\mathbf{u}}_d^s\\ \bar{\mathbf{q}}_n^s\end{Bmatrix}+\begin{bmatrix}-\mathbf{H}_d^{sc} & \mathbf{G}_n^{sc}\end{bmatrix}\begin{Bmatrix}\bar{\mathbf{u}}_d^v\\ \bar{\mathbf{q}}_n^v\end{Bmatrix}+[\mathbf{S}]_{\mathrm{DD}}\{\mathbf{Q}_{\mathrm{D}}\}$$
$$-[\bar{\mathbf{D}}]_{\mathrm{DD}}\{\dot{\mathbf{u}}_{\mathrm{D}}\}-\mathbf{u}_{\mathrm{D}} \tag{25}$$

The heat source inside the considered domain is omitted for facilitation, then combining Eq. (23) and Eq. (25), one gets:

$$\left(-[\bar{\mathbf{D}}]_{\mathrm{DD}}+\begin{bmatrix}-\bar{\mathbf{G}}_d^{ss} & \bar{\mathbf{H}}_n^{ss}\end{bmatrix}_{\mathrm{DB}}\mathbf{A}[\bar{\mathbf{D}}]_{\mathrm{BD}}\right)\{\dot{\mathbf{u}}_{\mathrm{D}}\}$$
$$=\mathbf{u}_{\mathrm{D}}+\left(\begin{bmatrix}-\bar{\mathbf{H}}_d^{ss} & \bar{\mathbf{G}}_n^{ss}\end{bmatrix}_{\mathrm{DB}}+\begin{bmatrix}-\bar{\mathbf{G}}_d^{ss} & \bar{\mathbf{H}}_n^{ss}\end{bmatrix}_{\mathrm{DB}}\mathbf{A}\begin{bmatrix}-\bar{\mathbf{H}}_{dd}^{ss} & \bar{\mathbf{G}}_{dn}^{ss}\\ -\bar{\mathbf{H}}_{nd}^{ss} & \bar{\mathbf{G}}_{nn}^{ss}\end{bmatrix}_{\mathrm{BB}}\right)\begin{Bmatrix}\bar{\mathbf{u}}_d^s\\ \bar{\mathbf{q}}_n^s\end{Bmatrix}$$
$$+\left(\begin{bmatrix}\mathbf{H}_d^{sv} & -\mathbf{G}_n^{sv}\end{bmatrix}_{\mathrm{DB}}+\begin{bmatrix}-\bar{\mathbf{G}}_d^{ss} & \bar{\mathbf{H}}_n^{ss}\end{bmatrix}_{\mathrm{DB}}\mathbf{A}\begin{bmatrix}-\mathbf{H}_{dd}^{sv} & \mathbf{G}_{dn}^{sv}\\ -\mathbf{H}_{nd}^{sv} & \mathbf{G}_{nn}^{sv}\end{bmatrix}_{\mathrm{BB}}\right)\begin{Bmatrix}\bar{\mathbf{u}}_d^v\\ \bar{\mathbf{q}}_n^v\end{Bmatrix} \tag{26}$$

For short, we further denote:

$$\mathbf{P}=-[\bar{\mathbf{D}}]_{\mathrm{DD}}+\begin{bmatrix}-\bar{\mathbf{G}}_d^{ss} & \bar{\mathbf{H}}_n^{ss}\end{bmatrix}_{\mathrm{DB}}\mathbf{A}[\bar{\mathbf{D}}]_{\mathrm{BD}}$$
$$\mathbf{B}=\mathbf{P}^{-1}\left(\begin{bmatrix}-\bar{\mathbf{H}}_d^{ss} & \bar{\mathbf{G}}_n^{ss}\end{bmatrix}_{\mathrm{DB}}+\begin{bmatrix}-\bar{\mathbf{G}}_d^{ss} & \bar{\mathbf{H}}_n^{ss}\end{bmatrix}_{\mathrm{DB}}\mathbf{A}\begin{bmatrix}-\bar{\mathbf{H}}_{dd}^{ss} & \bar{\mathbf{G}}_{dn}^{ss}\\ -\bar{\mathbf{H}}_{nd}^{ss} & \bar{\mathbf{G}}_{nn}^{ss}\end{bmatrix}_{\mathrm{BB}}\right)\begin{Bmatrix}\bar{\mathbf{u}}_d^s\\ \bar{\mathbf{q}}_n^s\end{Bmatrix}$$
$$+\mathbf{P}^{-1}\left(\begin{bmatrix}\mathbf{H}_d^{sv} & -\mathbf{G}_n^{sv}\end{bmatrix}+\begin{bmatrix}-\bar{\mathbf{G}}_d^{ss} & \bar{\mathbf{H}}_n^{ss}\end{bmatrix}_{\mathrm{DB}}\mathbf{A}\begin{bmatrix}-\mathbf{H}_{dd}^{sv} & \mathbf{G}_{dn}^{sv}\\ -\mathbf{H}_{nd}^{sv} & \mathbf{G}_{nn}^{sv}\end{bmatrix}\right)\begin{Bmatrix}\bar{\mathbf{u}}_d^v\\ \bar{\mathbf{q}}_n^v\end{Bmatrix} \tag{27}$$

Eq. (26) can be simplified into:

$$\dot{\mathbf{u}}_{\mathrm{D}}(t)=\mathbf{P}^{-1}\mathbf{u}_{\mathrm{D}}(t)+\mathbf{B}(t) \tag{28}$$

Eq. (28) is first-order ordinary differential equation. The solution process is introduced thoroughly in the following section.

4. The precise integration method

The complete solution of Eq. (28) is expressed as:

$$\mathbf{u}_{\mathrm{D}}=e^{\mathbf{P}^{-1}(t-t_0)}\mathbf{u}_{\mathrm{D}0}+\int_{t_0}^{t}e^{\mathbf{P}^{-1}(t-\tau)}\mathbf{B}(\tau)d\tau \tag{29}$$

In which

$$e^{\mathbf{P}^{-1}(t-t_0)}=\sum_n\frac{1}{n!}\left(\mathbf{P}^{-1}\right)^n\left(t-t_0\right)^n \tag{30}$$

Here, we call Eq. (30) the matrix exponential function. A scheme similar to quasi-initial condition method is employed to solve Eq. (29) for the purpose of reducing computation time:

$$\mathbf{u}_{\mathrm{D}k}=e^{(\mathbf{P}^{-1})\Delta t}\mathbf{u}_{\mathrm{D}(k-1)}+\int_{t_{k-1}}^{t_k}e^{(\mathbf{P}^{-1})(t_k-\tau)}\mathbf{B}(\tau)d\tau \tag{31}$$

where $\Delta t=t_k-t_{k-1}$ denotes the time step length. In general, we assume that the vector $\mathbf{B}(t)$ determined by the boundary condition, is steady and

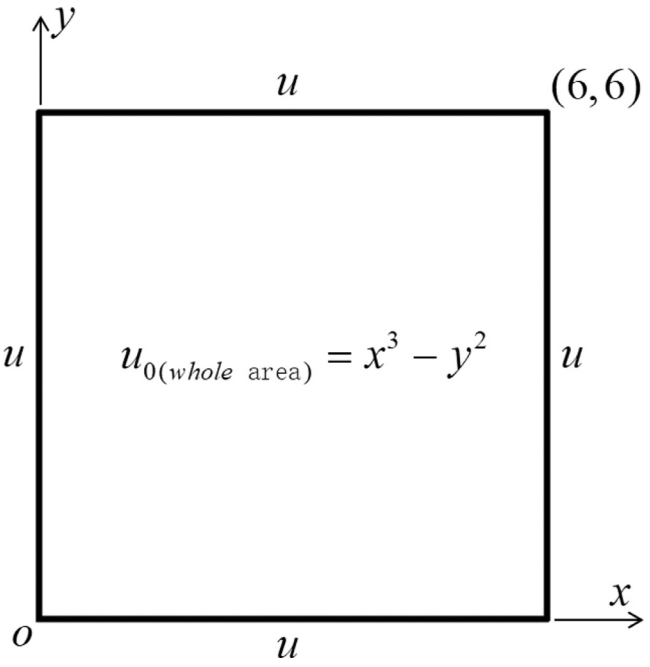

Fig. 3. Dirichlet problem with square: geometric model and conditions.

equals to $\mathbf{B}_k$ in the k-th time step. That is to say, the integrand vector $\mathbf{B}(t)$ is approximated by time constant interpolation. As a result, Eq. (31) is expressed as:

$$\mathbf{u}_{\mathrm{D}k}=e^{\Delta t(\mathbf{P})^{-1}}\mathbf{u}_{\mathrm{D}(k-1)}+\left((\mathbf{P})^{-1}\right)^{-1}(e^{\Delta t(\mathbf{P})^{-1}}-\mathbf{I})(\mathbf{P})^{-1}\Big(\begin{bmatrix}-\bar{\mathbf{H}}_d^{ss} & \bar{\mathbf{G}}_n^{ss}\end{bmatrix}_{\mathrm{DB}}$$
$$+\begin{bmatrix}-\bar{\mathbf{G}}_d^{ss} & \bar{\mathbf{H}}_n^{ss}\end{bmatrix}_{\mathrm{DB}}\mathbf{A}\begin{bmatrix}-\bar{\mathbf{H}}_{dd}^{ss} & \bar{\mathbf{G}}_{dn}^{ss}\\ -\bar{\mathbf{H}}_{nd}^{ss} & \bar{\mathbf{G}}_{nn}^{ss}\end{bmatrix}_{\mathrm{BB}}\Big)\begin{Bmatrix}\bar{\mathbf{u}}_d^s\\ \bar{\mathbf{q}}_n^s\end{Bmatrix}_k$$
$$+\left((\mathbf{P})^{-1}\right)^{-1}(e^{\Delta t(\mathbf{P})^{-1}}-\mathbf{I})(\mathbf{P})^{-1}\Big(\begin{bmatrix}\mathbf{H}_d^{sv} & -\mathbf{G}_n^{sv}\end{bmatrix}_{\mathrm{DB}}+\begin{bmatrix}-\bar{\mathbf{G}}_d^{ss} & \bar{\mathbf{H}}_n^{ss}\end{bmatrix}_{\mathrm{DB}}$$
$$\times\mathbf{A}\begin{bmatrix}-\mathbf{H}_{dd}^{sv} & \mathbf{G}_{dn}^{sv}\\ -\mathbf{H}_{nd}^{sv} & \mathbf{G}_{nn}^{sv}\end{bmatrix}_{\mathrm{BB}}\Big)\begin{Bmatrix}\bar{\mathbf{u}}_d^v\\ \bar{\mathbf{q}}_n^v\end{Bmatrix}_k \tag{32}$$

5. Numerical examples

Three numerical examples that possess analytical solutions and one engineering application are used to illustrate the stability, accuracy and convergence of the proposed DiPIBFM for solving 2-D transient heat conduction problems.

The relative error is used to study error estimation and convergence of the proposed method and defined as follows:

$$error=\frac{1}{|v^{(e)}|_{\max}}\sqrt{\frac{1}{M}\sum_{i=1}^{M}\left[v_i^{(e)}-v_i^{(n)}\right]^2} \tag{33}$$

where$|v^{(e)}|_{\max}$ is the maximum value of the exact solution over M sample points, and superscripts *e* and *n* denote the exact and numerical solutions, respectively.

5.1. Example 1

The first example is a problem with Dirichlet boundary conditions (BCs) on a square region and the size information is depicted in Fig. 3 (with length units in m). The heat conductivity *k*, heat capacity *c* and density ρ of the material is 1 W/m• °C, 1 J/kg• °C and 1 kg/m^2. The analytical solution of temperature *u* corresponding to this problem is expressed as:

$$u(x,y,t)=x^3-y^2+2t(3x-1) \tag{34}$$

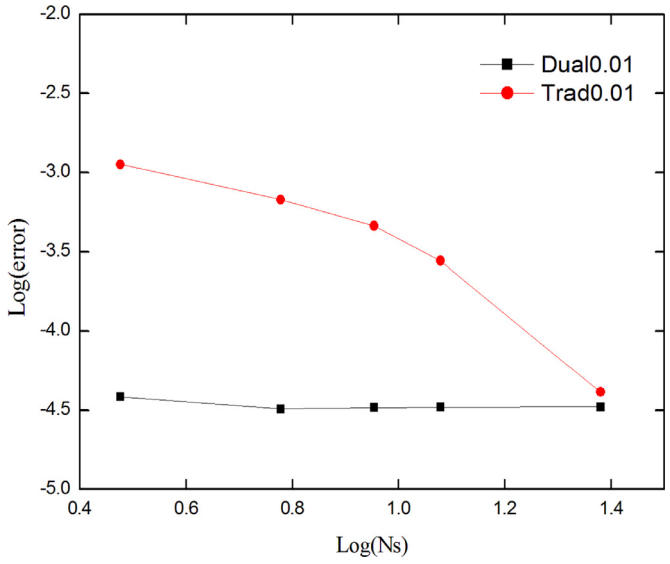

Fig. 4. Comparison of convergence for internal source nodes' u within the time interval [0 s, 0.01 s].

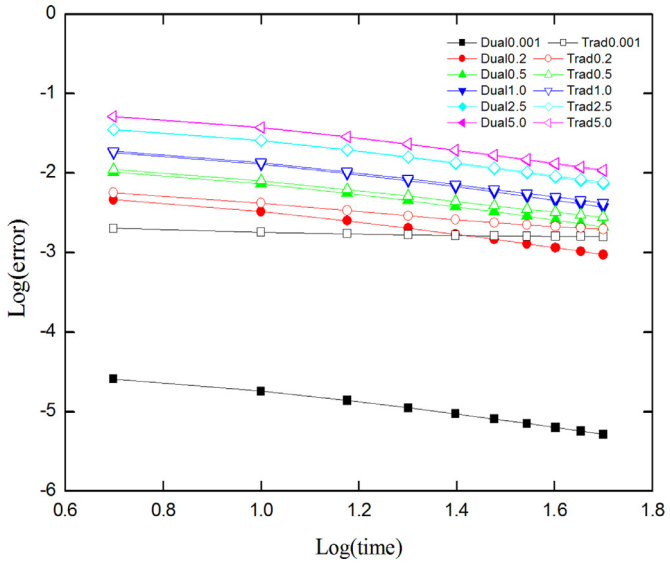

Fig. 5. Relative errors of u inside the considered domain along time within the time interval [0 s, 50 s].

The boundary condition u based on the above solution is specified along alledges. And only the 1-th time step's initial temperatures inside the considered domain are specified according to the above analytical solution, the other time step's initial potentials inside the domain are calculated by Eq. (26). It can be seen from Fig. 4, five sets of source points are employed on all edges, $n = 3$, 6, 9, 12, and 24. The number of nonconforming quadratic triangular elements inside the square and the internal source nodes is 62 and 372, respectively. Only one time step namely 0.01 s is applied in Fig. 4, and the time interval is [0 s, 0.01 s]. Fig. 4 shows the relative error of internal source nodes' computed temperature with employing these five sets of boundary source nodes.

Then the variation of temperatures inside the considered domain within the time interval [0 s, 50 s] is considered. Six sets of time steps are employed in this example, $\triangle t = 0.001$ s, 0.2 s, 0.5 s, 1.0 s, 2.5 s, and 5.0 s. Fig. 5 demonstrates the comparisons of accuracy for internal source nodes' computed temperature with employing these six sets of time steps. As illustrated in Figs. 5, when $\triangle t = 0.001$ s, the proposed method is two orders of magnitude higher than that of the traditional method. However, for other larger time step length, the advantage of our method is not obvious. The reasons are as follows: From Eqs. (15) and (31), we can see that the variation of physical variables with respect to space is interpolated by the dual interpolation elements, while the interpolation in time can be considered as constant interpolation. Thus, the relative error brought by interpolation in time will be smaller when the time step length approaches to zero, and the advantage of our proposed method, which has higher interpolation accuracy in space, will be shown, and Table 1 demonstrates the computer time consumed by DiPIBFM and PIBFM, it shows the efficiency of our new method.

Table 1
CPU time of one time step.

Dual0.001	10.096s
Trad0.001	9.398s

5.2. Example 2

Our second example is ahollow square with mixed boundary conditions. The dimensions of this structure are shown in Fig. 6(a). The conductivity k, heat capacity c and density ρ of the material is 1 W/m• °C, 1 J/kg• °C and 1 kg/m^2. And analytical solution for the 2-D transient heat transfer problem is selected as:

$$u(x, y, t) = x^2 + 2y^2 + 6t \tag{35}$$

The Dirichlet boundary conditions are specified on the circle and Neumann boundary conditions are specified on all outer straight edges corresponding to the above analytical solution (see Fig. 6(b)). In this implementation, 176 discontinuous quadratic triangular elements, 63 boundary source nodes, 1056 internal source nodes are employed. The time interval of the variation of temperatures is [0 s, 50 s]. And six sets of time steps, $\triangle t = 0.005$ s, 0.01 s, 0.2 s, 0.5 s, 1.0 s, and 2.5 s, are employed to demonstrate the convergence and stability of our proposed method along time.

In Fig. 7, we can easily find that the numerical results of physical variables u at internal source points convergent stably to analytical solution as the time step length becomes smaller and smaller. Since the S3 elements (see Section 2.1) were used in our proposed method, it achieves higher accuracy and faster convergence rates for the mixed boundary condition problem.

5.3. Example 3

In the third example, to testify the power of our proposed method, we concern a square thattakes the area [0 mm, 6 mm] × [0 mm, 6 mm] with the following boundary and initial conditions (see Fig. 8). The conductivity k, heat capacity c and density ρ of the material is 1 W/m• °C, 1 J/kg• °C and 1 kg/m^2. The analytical solution used is defined as:

$$\begin{aligned} u(x, y, t) &= \sum_{n=1}^{\infty}\sum_{j=1}^{\infty} A_n \sin\frac{n\pi x}{6}\sin\frac{j\pi y}{6}\exp\left[-\left(\frac{n^2\pi^2}{36}+\frac{j^2\pi^2}{36}\right)t\right] \\ &\approx \sum_{n=1}^{100}\sum_{j=1}^{100} A_n \sin\frac{n\pi x}{6}\sin\frac{j\pi y}{6}\exp\left[-\left(\frac{n^2\pi^2}{36}+\frac{j^2\pi^2}{36}\right)t\right] \end{aligned} \tag{36}$$

where

$$A_n = \frac{120}{nj\pi^2}\left[(-1)^n - 1\right]\left[(-1)^j - 1\right] \tag{37}$$

In this implementation, 62 discontinuous quadratic triangular elements, 36 boundary nodes, 372 domain nodes are employed. The time interval of the variation of temperatures is [0 s, 9.6 s]. And five sets

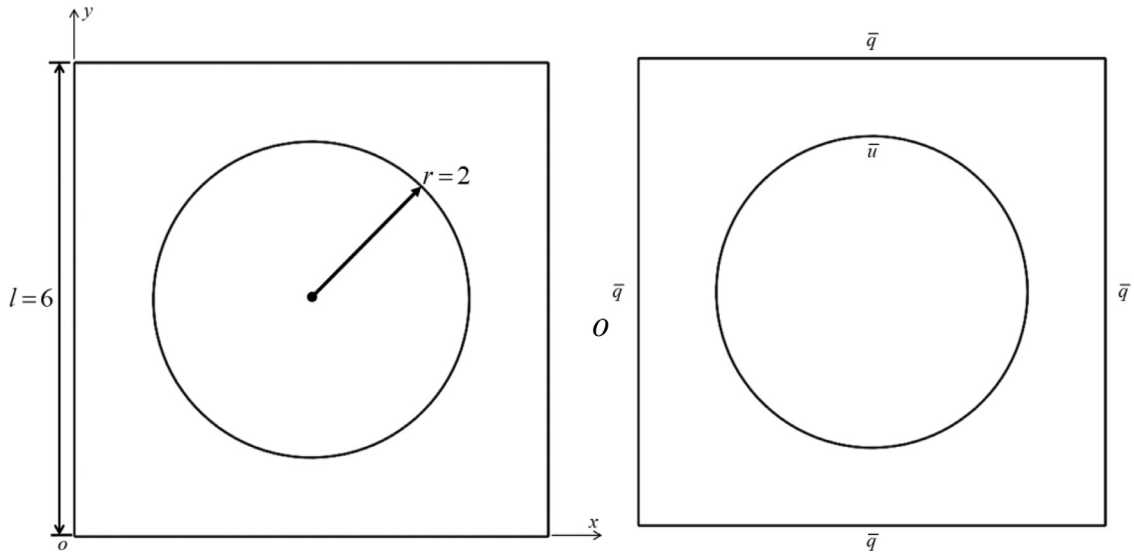

Fig. 6. Mixed problem on hollow square: (a) geometric model and (b) boundary conditions.

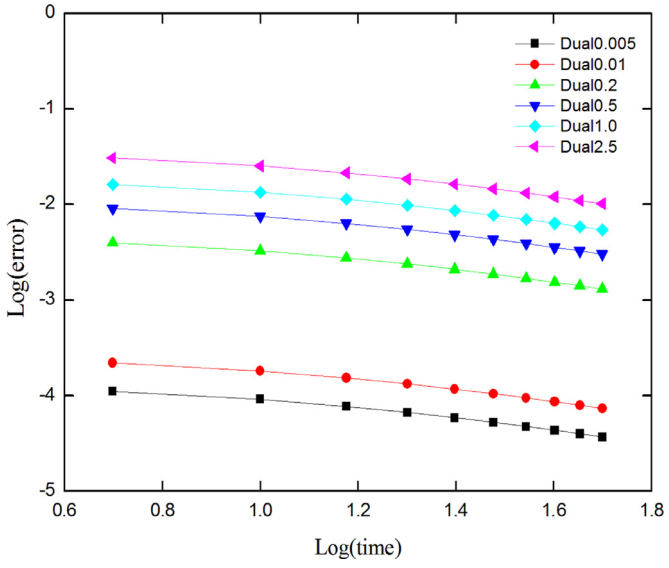

Fig. 7. Relative errors of u inside the considered domain along time within the time interval [0 s, 50 s].

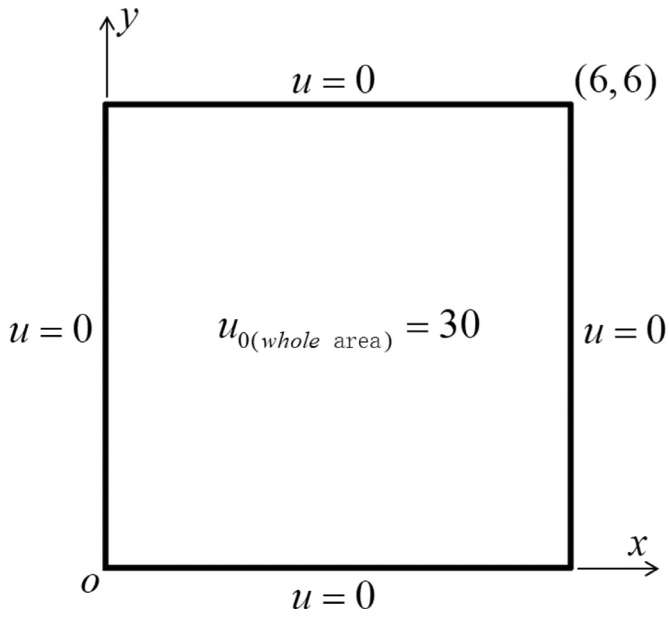

Fig. 8. Mixed problem with square: geometric model and conditions.

Table 2
Coordinates of sample nodes.

Nodes	Location
P1	(0.19509, 5.500965)
P2	(3.50006, 3.013105)

of time steps are employed in this example, $\triangle t$ = 0.001 s, 0.1 s, 0.2 s, 0.4 s, 0.8 s. The temperature variation history at 2 internal source nodes inside the considered domain namely P1, P2 the location of which are shown in Table 2 is concerned, for the purpose of studying the stability and accuracy of our proposed method distinctly. The numerical results of sample nodes are listed in Table 3 and Table 4 and the computed physical variables u (shown as solid dots) at these two sample nodes are compared with that in analytical solution (shown as lines) in Fig. 9.

Table 3
Temperatures of P1.

Time (s)	Analytical solution	$\triangle t$ = 0.001	$\triangle t$ = 0.1	$\triangle t$ = 0.2	$\triangle t$ = 0.4	$\triangle t$ = 0.8
0.8	1.12810	1.12676	1.12676	1.12676	1.12676	1.12676
1.6	0.56353	0.56332	0.56332	0.56332	0.56332	0.56332
2.4	0.34701	0.34684	0.34684	0.34684	0.34684	0.34684
3.2	0.22198	0.22187	0.22187	0.22187	0.22187	0.22187
4.0	0.14296	0.14290	0.14290	0.14290	0.14290	0.14290
4.8	0.09217	0.09215	0.09215	0.09215	0.09215	0.09215
5.6	0.05944	0.05943	0.05943	0.05943	0.05943	0.05943
6.4	0.03833	0.03833	0.03833	0.03833	0.03833	0.03833
7.2	0.02472	0.02473	0.02473	0.02473	0.02473	0.02473
8.0	0.01594	0.01595	0.01595	0.01595	0.01595	0.01595
8.8	0.01028	0.01029	0.01029	0.01029	0.01029	0.01029
9.6	0.00663	0.00663	0.00663	0.00663	0.00663	0.00663

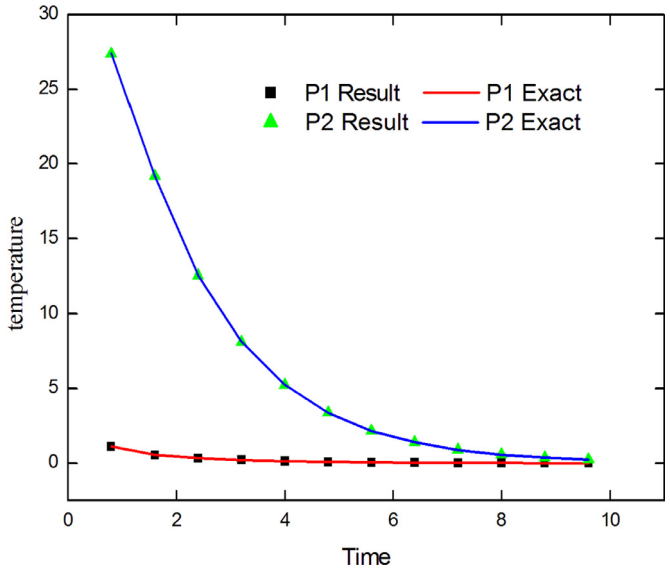

Fig. 9. Comparison between numerical results and exact solutions.

From Table 3, Table 4 and Fig. 9, it is very interesting that nearly the same results can be obtained by employing different time steps, the reason is as follows: The Dirichlet boundary condition, which is equal to zero, is time-independent in this example with each time step. The relative error is mainly brought by the interpolation of unknown boundary normal fluxes q and the interpolation of first derivatives of the $u(\mathbf{x}, t)$ versus time variable t. This example testifies the DiPIBFM has high rates of convergence. The agreement between numerical results and analytical solution is good.

Table 4
Temperatures of P2.

Time (s)	Exact solution	$\triangle t = 0.001$	$\triangle t = 0.1$	$\triangle t = 0.2$	$\triangle t = 0.4$	$\triangle t = 0.8$
0.8	27.38134	27.37102	27.37102	27.37102	27.37102	27.37102
1.6	19.20145	19.18873	19.18873	19.18873	19.18873	19.18873
2.4	12.56216	12.55760	12.55760	12.55760	12.55760	12.55760
3.2	8.12148	8.12021	8.12021	8.12021	8.12021	8.12021
4.0	5.23984	5.23986	5.23986	5.23986	5.23986	5.23986
4.8	3.37946	3.37997	3.37997	3.37997	3.37997	3.37997
5.6	2.17947	2.18011	2.18011	2.18011	2.18011	2.18011
6.4	1.40556	1.40617	1.40617	1.40617	1.40617	1.40617
7.2	0.90645	0.90698	0.90698	0.90698	0.90698	0.90698
8.0	0.58458	0.58500	0.58500	0.58500	0.58500	0.58500
8.8	0.37700	0.37733	0.37733	0.37733	0.37733	0.37733
9.6	0.24313	0.24337	0.24337	0.24337	0.24337	0.24337

5.4. Example 4

Our forth example is a transient heat transfer problem on a real dam structure (see Fig. 10). The length of the contact surface between the dam and the foundation is 49 m. The real dam's left side is 65 m in height, adjoining the upstream, and the dam's right side is exposed to air. Besides, the upstream water level is the same as the height of the dam's left side. The conductivity k, heat capacity c and density ρ of the material is 9.75 kJ/m•h• °C, 0.888 kJ/kg• °C and 2539 kg/m^2.

The bed rock's temperature is 0 °C and the air temperature is 10.3 °C (see Fig. 8). The initial condition of the real dam is 27 °C and the water keeps a constant temperature which is equal to 13.4 °C.

As observed in Fig. 11, Fig. 12 and Fig. 13, the temperature distribution over the considered domain along time of our method convergents stably to temperature cloud picture of FEM. The results of DiPIBFM is calculated by our proposed method using 479 discontinuous linear triangular elements (1437 domain nodes) and 69 boundary nodes,. The

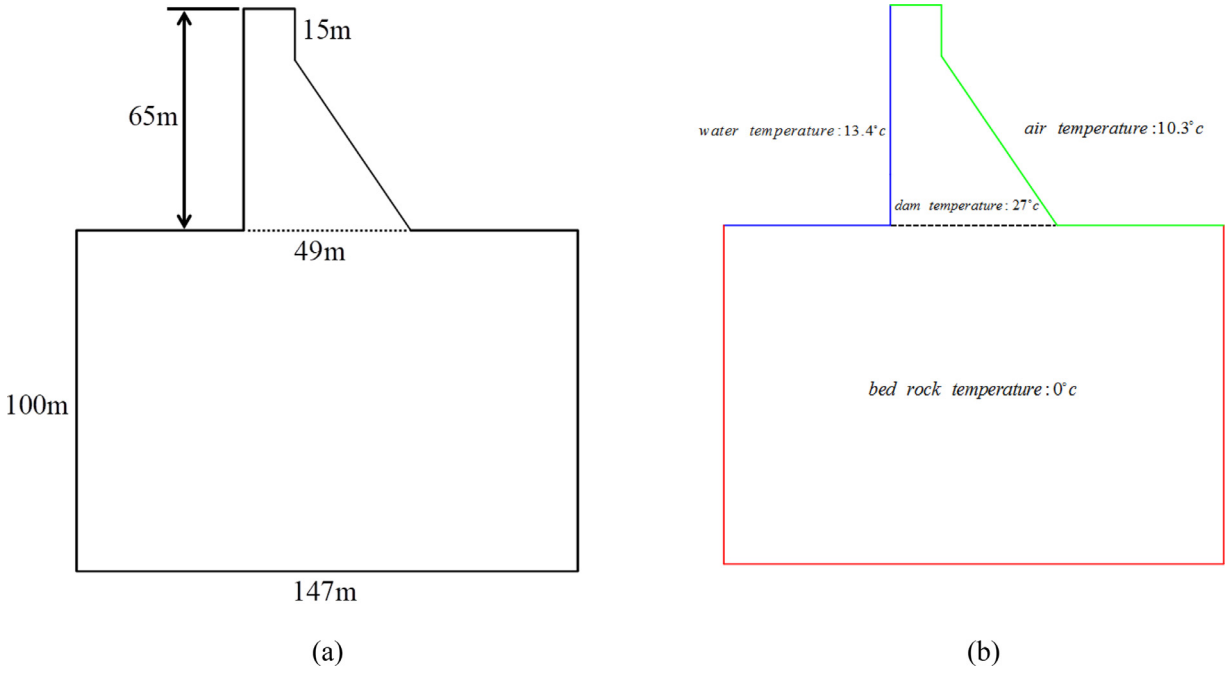

Fig. 10. Transient heat conduction problem on a dam: (a) geometry and (b) boundary conditions.

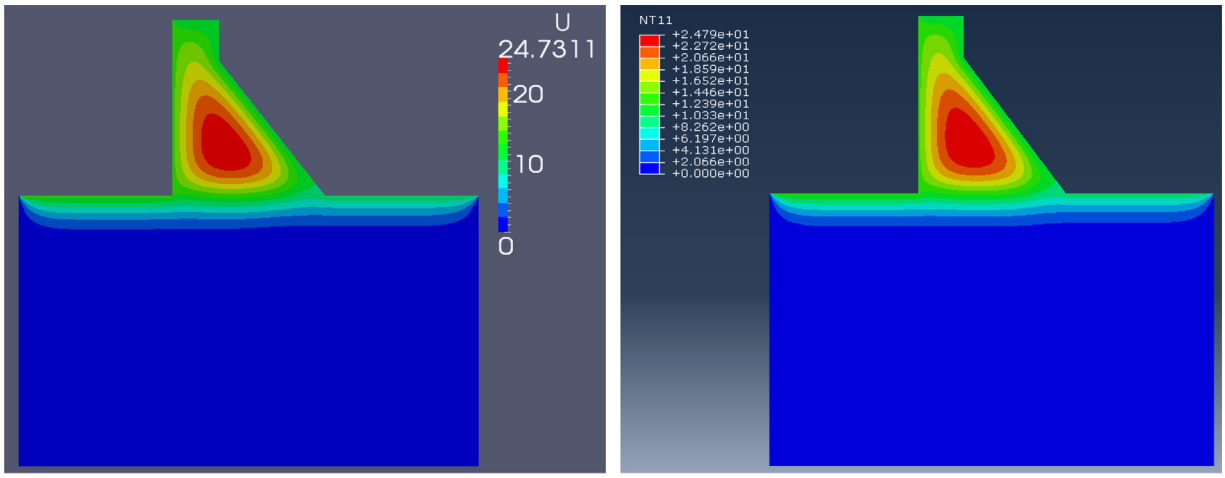

Fig. 11. Potential distribution (t = 1 year) computed by: (a) DiPIBFM and (b) FEM.

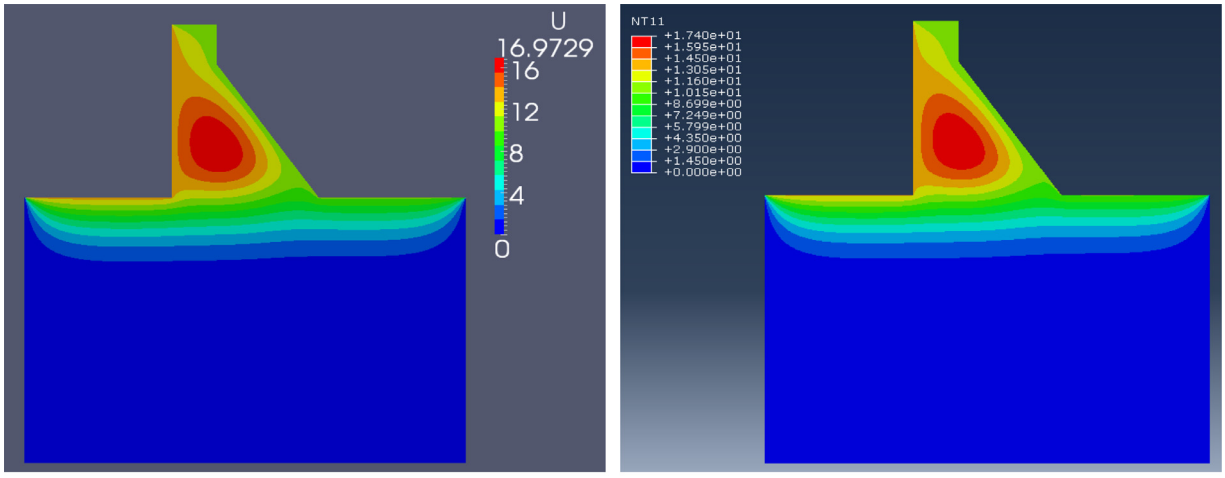

Fig. 12. Potential distribution (t = 3 year) computed by: (a) DiPIBFM and (b) FEM.

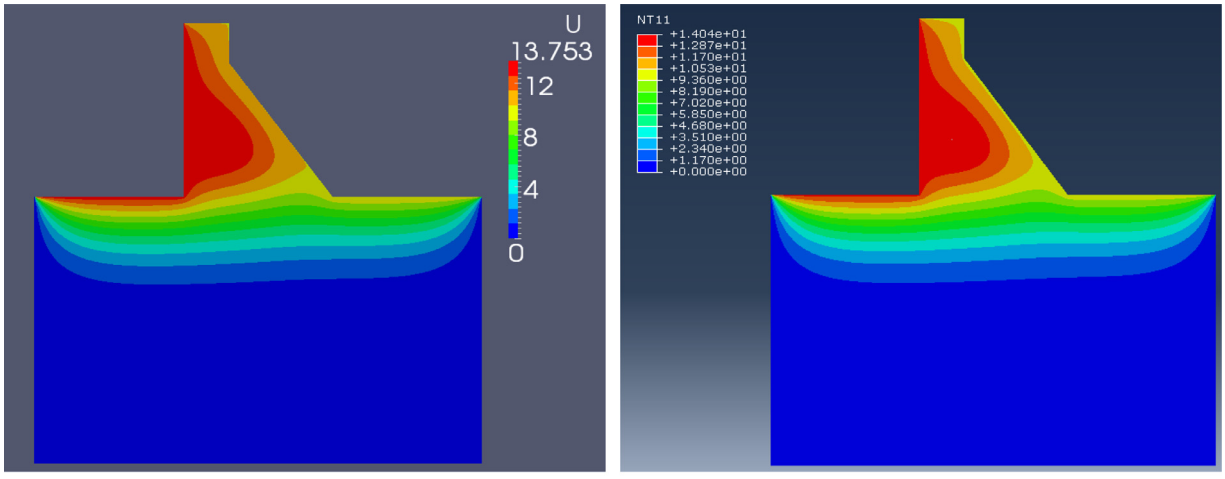

Fig. 13. Potential distribution (t = 5 year) computed by: (a) DiPIBFM and (b) FEM.

numerical result calculated by the FEM with 177,501 source pointsis used as reference solution.

6. Conclusions

In this paper, the precise integration method which has broader application prospect in many fields, such as heat transfer problems and structure dynamic problems etc., has been enhanced by coupling the dual interpolation boundary face method, and a new combined algorithm (DiPIBFM) is presented for solving two-dimensional transient heat conduction problems. Furthermore, based on the advantages of PIM and DiBFM, the DiPIBFM can achieve higher accuracy and is better suitable to solve structural dynamics with applying smaller time step. As a result, when compared with the conventional precise integration BEM, the DiPIBFM can approximate both conforming and nonconforming fields more freely and precisely. All presented numerical examples verify the stability and accuracy of our method when solving transient heat conduction problems with different types of boundary condition.

This research just studies the performance of the proposed method when applying to 2D heat transfer problem. Extensions of the DiPIBFM to solve other time domain problems are possible and seductive, because of the advantages of DiPIBFM: (i) it uses the time-independent fundamental solution, thus, the accuracy and the stability of integration is higher than methods that implement with the time-dependent fundamental solution; (ii) it improves the interpolation precision and eliminates the geometry error, it also has the potential to increase the accuracy when it is applied to structural dynamics or other difficult transient problems. In future work, we plan to extend the range of applicability of the method to the three-dimensional case. Work along this line is underway.

Declaration of Competing Interest

None.

Acknowledgments

This work was supported by the National Natural Science Foundation of China under Grant No. 11972010 and 11772125.

References

[1] Tao WQ. Numerical heat transfer, Xi'an: Xi'an Jiaotong University Press; 1988. (In Chinese).
[2] Tao WQ, He YL, Li ZY, Qu ZG. Some recent advances in finite volume approach and their applications in the study of heat transfer enhancement. Int Therm Sci 2005;44(7):623–43.
[3] Lewis RW, Morgan K, Thomas HR, et al. The finite element method in heat transfer analysis. Wiley; 1996.
[4] Liu YJ. Fast multipole boundary element method - theory and applications in engineering. Cambridge: Cambridge University Press; 2009.
[5] Zhang JM, Qin XY, Han X. A boundary face method for potential problems in three dimensions. Int J Numer Methods Eng 2009;80:320–37.
[6] Sutradhar A, Paulino GH, Gray L, J. Transient heat conduction in homogeneous and non-homogeneous materials by the Laplace transform Galerkin boundary element method. Eng Anal Bound Elem 2002;26:119–32.
[7] Guo SP, Zhang JM, Li GY, et al. Three dimensional transient heat conduction analysis by Laplace transformation and multiple reciprocity boundary face method. Eng Anal Bound Elem 2013;37:15–22.
[8] Ibanez MT, Power H. An efficient direct BEM numerical scheme for heat transfer problems using Fourier series. Int J Numer Methods Heat Fluid Flow 2000;10:687–720.
[9] Gupta A, Sullivan JM, Delgado HE. An efficient BEM solution for three dimensional transient heat conduction. Int J Numer Methods Heat Fluid Flow 1995;5:327–40.
[10] Wang CH, Grigoriev MM, Dargush GF. A fast multi-level convolution boundary element method for transient diffusion problems. Int J Numer Methods Eng 2005;62:1895–926.
[11] Thaler RH, Mueller WK. A new computational method for transient heat conduction in arbitrarily shaped regions. Fourth international heat transfer conference. Amsterdam: Elsevier Publishing Co; 1970.
[12] Brebbia CA, Telles JCF, Wrobel LC. Boundary element techniques: theory and applications in engineering. Berlin and New York: Springer-Verlag; 1984.
[13] Zhou Fenglin, You Yulong, Li Guang, Xie Guizhong, Li Guang. The precise integration method for semi-discretized equation in the dual reciprocity method to solve three-dimensional transient heat conduction problems. Eng Anal Bound Elem 2018;95:160–6.
[14] Zhong WX. On precise time-integration method for structural dynamics. J Dalian Univ Tech 1994;24(2):131–6 (In Chinese).
[15] Zhang JM, Han L, Lin WC, Dong YQ, Ju CM. A new implementation of BEM by an expanding element interpolation method. Eng Anal Bound Elem 2017;78:1–7.
[16] Zhang JM, Dong YQ, Lin WC, Ju CM. A singular element based on dual interpolation BFM for V-shaped notches. Appl Math Model 2019;71:208–22.
[17] Zhang JM, He R, Chi BT, Lin WC. A dual interpolation boundary face method with Hermite-type approximation for potential problems. Appl Math Model 2020;81:457–72.
[18] Zhang JM, Chi BT, Lin WC, Ju CM. A dual interpolation boundary face method for three-dimensional potential problems. Int J Heat Mass Transf 2019;140:862–76.
[19] Zhang JM, Lin WC, Dong YQ. A double-layer interpolation method for implementation of BEM analysis of problems in potential theory. Appl Math Model 2017;51:250–69.
[20] Lancaster P, Salkauskas K. Surface generated by moving least squares methods. Math Comput 1981;37:141–58.